Biologically Inspired Modeling of Smart Grid for Dynamic Power-Flow Control

Hidefumi Sawai[1], Hideaki Suzuki[1], and Hiroyuki Ohsaki[2]

[1] National Institute of Information and Communications Technology, Japan
{sawai,hsuzuki}@nict.go.jp
[2] Graduate School of Osaka University, Suita 565-0871 Japan
oosaki@ist.osaka-u.ac.jp

Abstract. Smart grid is an electric power network which enables an effective use of electric power in a highly parallel distributed manner. We have first formulated the basic equations for the smart grid by inspiring from the mechanisms in biological organism, and controled the power-flow dynamically in the smart grid by monitoring an objective function, which reflects the power-flow and the constraint imposing on the power nodes. To validate the operation of the smart grid, we performed several simulation experiments: which include the operations of a conventional power network, a microgrid (comprises eight power nodes), and a smart grid (comprises three microgrids integrated into the conventional power network) both in *synchronous and asynchronous manners* for the operation of power nodes. Furthermore, even for the case of power failure such as outage, power recovery can be automatically achieved through bypass connections similar to synaptic interconnections in a dynamic function of brain. This kind of flexible function in the smart grid makes it possible to promote the introduction of renewable energy, such as solar energy, wind energy, and biomass energy rather than fossil energy.

Keywords: smart grid, dynamic control, highly distributed asynchronous system, synaptic connection, brain function.

1 Introduction

Smart grid is an intelligent power network which recently attracted a lot of attention because it enables many things to positively affect the environment on the Earth[3]-[13]. Fig.1 shows the evolution from a conventional power network (a) to a smart grid with microgrids (b)[5]. The conventional power network is generally a commercial network which includes power plants, power generators, and power networks connected to demand sites. This network is very reliable and robust against a small accident in a local area. In reality, there were no experiences of outage except for a large-scale disaster in Japan. On the other hand, from the viewpoint of an efficient use of energy on the demand side, as a simultaneous use of electric and thermal energy increases an integrated power-efficiency, i.e, reducing energy costs for users on the demand side, many on-site

J. Suzuki and T. Nakano (Eds.): BIONETICS 2010, LNICST 87, pp. 111–127, 2012.

distributed power supplies have already been introduced in the neighborhood of the demand sites. Furthermore, very recently, from the viewpoint of prevention against the global warming, the power plant systems based on renewable energy such as solar energy, wind energy, and biomass energy have been introduced. This situation is shown in Fig.1(b). In this figure, many power supplies including batteries or storages, and demand sides are distributed in the microgrid power networks and integrated into the conventional power network through the transformer and distribution substations as a whole power system. There are many *pro-and-cons* on the introduction of smart grid: for examples, it is not observable nor controllable from the conventional power networks, an increase of demand on the power efficiency on the demand sides, and the balance between them should be adjusted. However, we should plan to complimentarily promote the symbiosis between the smart grid and the conventional power network for the future of the Earth.

The microgrid basically comprises (a)power (both electric and thermal) supplies, (b)power storage equipments, (c)power network, (d) a control system based on IT (Information Technology), and (e)power demand. The big difference between the commercial power network and smart grid is the application of thermal energy, and the existence of power storages, especially batteries. As the number of demand sites in the microgrid is small, and the fluctuation in power supply becomes large, the power-flow control should be adequately operated in real-time. Also, as the power supply itself is unstable due to the climate change in the case of natural energy such as solar energy and wind energy, it is always necessary to improve the energy supply. The previous studies, e.g., the paper[10] overviews several areas of computational intelligence techniques in the smart grid of the future. The paper[12] claimed computational intelligence for smart grid without showing any concrete methods, and the paper[13] focused on the automatic electiric load detection. The paper[11] proposed a domestic energy management methodology for optimizing efficiency in smart grid. In this paper, we will show a dynamic control method of power-flow in microgrids and then integrate them into a public (infrastructural) power network using simulation experiments including a power failure such as outage. Even in such an unusual situation, we will show that automatic recovery of power supply will be achieved through bypass connections.

These kinds of situations for the smart grid to dynamically adapt to a changing environment would remind us of the corresponding biological functions in several hierarchical levels, which include: (1)a gene regulatory network for the metabolism of a cell[1] in the micro-level for responding to the demand in microgrid. (2)each power node could be regarded as each neuron in a brain network[2], and the change of synaptic plasticity between neurons would correspond to the switching of power supply between the power nodes. (3)If we regard each microgrid as each cell in a biological creature, some microgrids would form a multi-cell creature, and the smart grid would form an eco-system in the macro-level whose network architecture would always adapt to a dynamically changing environment. (4)the evolution of life would correspond to the evolution of smart grid[5],

where each power node (usually *alive* and sometimes *dead*) seems to behave like each agent or individual in a macroscopic eco-system.

The above mentioned analogical inspiration would lead us to design the architectures and analyse the functions of a smart grid in the later sections.

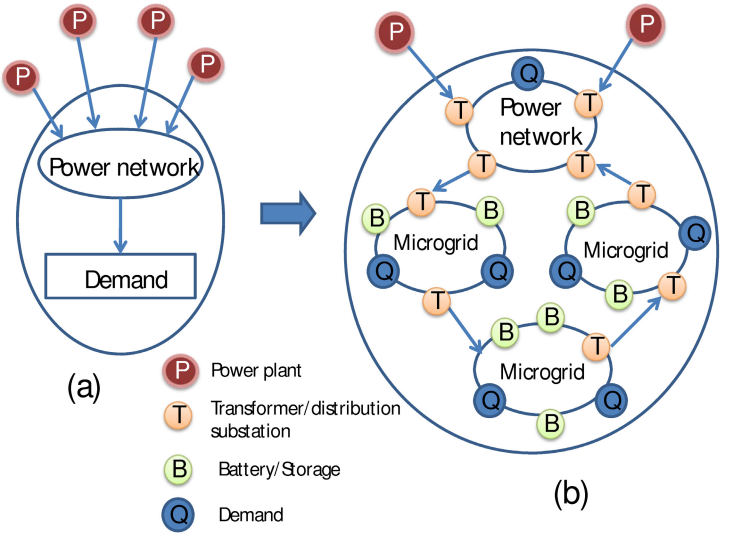

Fig. 1. Evolution of smart grid power network[5]

2 Microgrid Power Network

2.1 Basic Power-Flow Equations

The basic equations for the microgrid power network shown in Fig.2 are defined as follows. This network architecture can adapt to any situation in the microgrid without loss of generality.

$$B_j(t) = \sum_i w_{ij}(t)P_i(t) + \sum_{j'} w_{j'j}(t)B_{j'}(t), \tag{1}$$

$$B_{j'}(t) = \sum_i w_{ij'}(t)P_i(t), \tag{2}$$

$$Q_k(t) = \sum_j w_{jk}(t)B_j(t) + \sum_i w_{ik}(t)P_i(t) + \sum_{j'} w_{j'k}(t)B_{j'}(t), \tag{3}$$

where, $B_j(t)$ is the power in the j^{th} battery or storage node, and $B_{j'}(t)$ is the power in the j'^{th} battery or storage node which interconnects with $B_j(t)$. $P_i(t)$ is

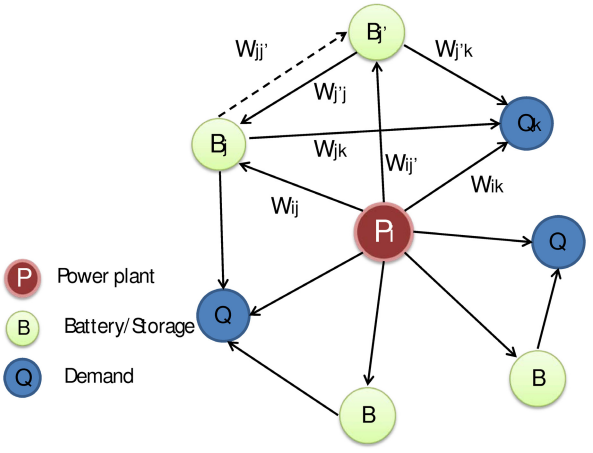

Fig. 2. Model of microgrid power network

the power in the i^{th} power plant. The interconnection $w_{ij}(t)$ between the nodes $P_i(t)$ and $B_j(t)$ represents the power-flow ratio between 0 and 1 for the two nodes. $Q_k(t)$ is the power at the k^{th} demand node. The interconnection $w_{jk}(t)$ represents the power-flow ratio for nodes $B_j(t)$ and $Q_k(t)$.

2.2 Objective Function

The *nonlinear* and *time-varing* objective function $R(t)$ to be minimized can be defined as follows:

$$R(t) \equiv P_0(t) + \lambda H_p^*(t) + \mu H_v^*(t) + \nu H_e^*(t) + \xi H_s^*(t), \tag{4}$$

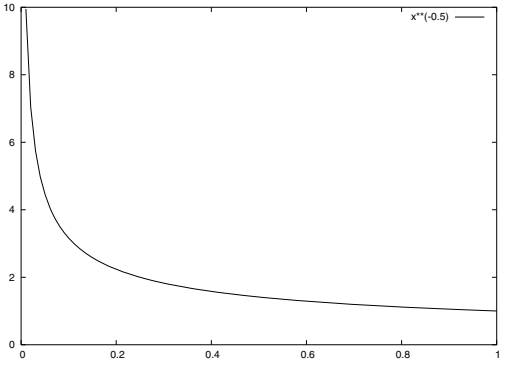

Fig. 3. Constraint function $H_p(t)$ for power plant

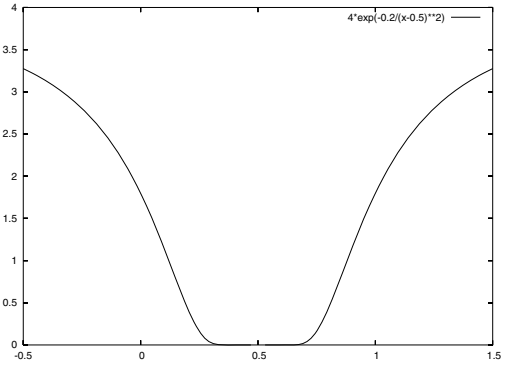

Fig. 4. Constraint functions $H_B(t)$ and $H_Q(t)$ common to transformer and distribution substations and demand nodes

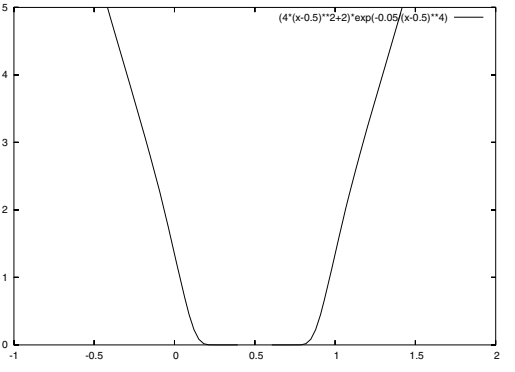

Fig. 5. Constraint function $H_e(t)$ for power supply

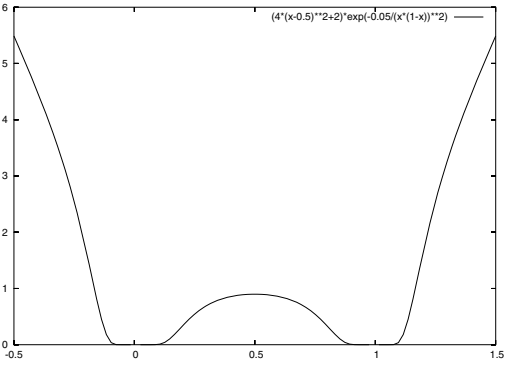

Fig. 6. Constraint function $H_s(t)$ for switching

where λ, μ, ν, and ξ are constants, and $P_0(t)$ is the total of each fuel cost $f(P_i(t))$ in each power plant, approximated as a quadratic function of $P_i(t)$:

$$P_0(t) \equiv \sum_i f(P_i(t)) = \sum_i (a_i + b_i P_i(t) + c_i P_i^2(t)),$$

where, a_i, b_i, c_i are positive constants. $H_p^*(t)$ is defined as a function concerning the power plants P, where $H_p(P_i(t))$ is a function that should satisfy the positive power generation constraint at the power plant, as shown in Fig.3.

$$H_p^*(t) \equiv \sum_i H_p(P_i(t)) = \sum_i P_i(t)^{-\alpha_p}, \alpha_p = const.$$

$H_v^*(t)$ is the combinational function of the constraint functions $H_B(t)$, $H_{B'}(t)$ and $H_Q(t)$. Functions $H_B(t)$, $H_{B'}(t)$ and $H_Q(t)$ should satisfy the capacity and demand, respectively, in the battery or storage B and demand Q.

$$\begin{aligned} H_v^*(t) \equiv & \sum_j H_B(B_j(t); B_j^{max}, B_j^{min}) + \sum_j H_{B'}(B_{j'}(t); B_{j'}^{max}, B_{j'}^{min}) \\ & + \sum_k H_Q(Q_k(t); Q_k^{max}, Q_k^{min}). \end{aligned}$$

These functions are *well-shaped* functions, as shown in Fig.4, and they determine the upper and lower limits of power capacity as shown below:

$$\begin{aligned} H_B(t) \equiv & \alpha_B exp\{-\beta_B/(B_j(t) - \gamma_B)^2\}, \\ & where, \alpha_B = const., \beta_B = 3(B_j^{max} - B_j^{min})^2/8, \gamma_B = (B_j^{min} + B_j^{max})/2, \\ H_Q(t) \equiv & \alpha_Q exp\{-\beta_B/(Q_k(t) - \gamma_B)^2\}, \end{aligned}$$

where, α_Q = constant. β_B and γ_B are determined if two flection points in the above-mentioned functions correspond to the minimum B_j^{min} and maximum B_j^{max} values of $B_j(t)$.

Next, we define an edge-constraint function $H_e^*(t)$ as follows:

$$H_e^*(t) \equiv \sum_i H_e(W_i(t)) + \sum_j H_e(W_j(t)) + \sum_{j'} H_e(W_{j'}(t)),$$

where,

$$0 \le W_i(t) = \sum_j w_{ij}(t) \le 1, 0 \le W_j(t) = \sum_k w_{jk}(t) \le 1, 0 \le W_{j'}(t) = \sum_k w_{j'k}(t) \le 1,$$

$$0 \le w_{ij}(t) = c_{ij} x_{ij}(t) \le 1, 0 \le w_{jk}(t) = c_{jk} x_{jk}(t) \le 1, 0 \le w_{j'k}(t) = c_{j'k} x_{j'k}(t) \le 1,$$

$$0 \le c_{ij}, c_{jk}, c_{j'k} \le 1, 0 \le x_{ij}(t), x_{jk}(t), x_{j'k}(t) \le 1,$$

where, the edge constraint function $H_e(W_i)$ is defined as a well-shaped function as shown in Fig.5; whose mathematical forms are as follows:

$$\begin{aligned} H_e(W_i(t)) \equiv & \alpha_e(W_i(t)) exp\{-\beta_e/(W_i(t)-\gamma_e)^4\}, \\ \alpha_e(x(t)) = & 4(x(t)-0.5)^2+2, \beta_e = 0.05, \gamma_e = 0.5. \end{aligned}$$

$H_e(W_i(t))$ is the function used to satisfy the condition that the total power limits the total flow produced by the power plant $P_i(t)$, as shown in Fig.5. Similarly, $H_e(W_j(t))$ is used to satisfy the condition that the total power limits the total flow produced by the battery or storage $B_j(t)$, and so on.

Next, we define the switching function $H_s^*(t)$ as shown in Fig.6, which represents the tendency toward two different switching modes, i.e., ON(0) and OFF(1), as follows:

$$\begin{aligned} H_s^*(t) \equiv & \sum_i \sum_j \alpha_s(x_{ij}(t)) exp[-\beta_s/\{x_{ij}^2(t)(1-x_{ij}(t))^2\}] \\ & + \sum_j \sum_k \alpha_s(x_{jk}(t)) exp[-\beta_s/\{x_{jk}^2(t)(1-x_{jk}(t))^2\}] \\ & + \sum_i \sum_k \alpha_s(x_{ik}(t)) exp[-\beta_s/\{x_{ik}^2(t)(1-x_{ik}(t))^2\}] \\ & + \sum_i \sum_{j'} \alpha_s(x_{ij'}(t)) exp[-\beta_s/\{x_{ij'}^2(t)(1-x_{ij'}(t))^2\}] \\ & + \sum_{j'} \sum_j \alpha_s(x_{j'j}(t)) exp[-\beta_s/\{x_{j'j}^2(t)(1-x_{j'j}(t))^2\}] \\ & + \sum_{j'} \sum_k \alpha_s(x_{j'k}(t)) exp[-\beta_s/\{x_{j'k}^2(t)(1-x_{j'k}(t))^2\}], \\ where, & \alpha_s(x) = 4(x-0.5)^2+2, \beta_s = const., \\ & 0 \le w_{ij}(t) = c_{ij}x_{ij}(t) \le 1, 0 \le w_{jk}(t) = c_{jk}x_{jk}(t) \le 1, \\ & 0 < c_{ij}, c_{jk} \le 1, 0 \le x_{ij}(t), x_{jk}(t) \le 1, etc., \end{aligned}$$

where c_{ij} is the coefficient of power-flow from node i to node j, and $x_{ij}(t)$ represents the switching value between the power nodes i and j.

The change in power $\Delta P_i(t)$ is calculated by

$$\Delta P_i(t) = -\eta \frac{\partial R(t)}{\partial P_i(t)} = -\eta \{ \frac{\partial P_0(t)}{\partial P_i(t)} + \lambda \frac{\partial H_p^*(t)}{\partial P_i(t)} + \mu \frac{\partial H_v^*(t)}{\partial P_i(t)} \}, \tag{5}$$

where,

$$\frac{\partial P_0(t)}{\partial P_i(t)} = b_i + 2c_i P_i(t), \frac{\partial H_p^*(t)}{\partial P_i(t)} = -\alpha_p P_i(t)^{-\alpha_p - 1}, \alpha_p = const.,$$

$$\frac{\partial H_v^*(t)}{\partial P_i(t)} = \frac{\partial H_B^*(t)}{\partial P_i(t)} + \frac{\partial H_{B'}^*(t)}{\partial P_i(t)} + \frac{\partial H_Q^*(t)}{\partial P_i(t)},$$

$$\frac{\partial H_B^*(t)}{\partial P_i(t)} = \sum_j \frac{\partial H_B(t)}{\partial B_j(t)} \{ \frac{\partial B_j(t)}{\partial P_i(t)} + \sum_{j'} \frac{\partial B_j(t)}{\partial B_{j'}(t)} \frac{\partial B_{j'}(t)}{\partial P_i(t)} \}$$

$$= \delta_j(t)(w_{ij}(t) + \sum_{j'} w_{j'j}(t) w_{ij'}(t)), \delta_j(t) \equiv \frac{\partial H_B(t)}{\partial B_j(t)},$$

$$\frac{\partial H_Q^*(t)}{\partial P_i(t)} = \sum_k \frac{\partial H_Q(t)}{\partial Q_k(t)} \{ \frac{\partial Q_k(t)}{\partial P_i(t)} + \sum_j \frac{\partial Q_k(t)}{\partial B_j(t)} (\frac{\partial B_j(t)}{\partial P_i(t)} + \sum_{j'} \frac{\partial B_j(t)}{\partial B_{j'}(t)} \frac{\partial B_{j'}(t)}{\partial P_i(t)})$$

$$+ \sum_{j'} \frac{\partial Q_k(t)}{\partial B_{j'}(t)} \frac{\partial B_{j'}(t)}{\partial P_i(t)} \}$$

$$= \sum_k \delta_k(t) \{ w_{ik}(t) + \sum_j w_{jk}(t)(w_{ij}(t) + \sum_{j'} w_{j'j}(t) w_{ij'}(t)) + \sum_{j'} w_{j'k}(t) w_{ij'}(t) \},$$

$$where, \delta_k(t) \equiv \frac{\partial H_Q(t)}{\partial Q_k(t)}.$$

Next, the change in the switching values $\Delta x_{jk}(t)$ can be calculated as follows:

$$\begin{aligned}
\Delta x_{jk}(t) &= -\eta \frac{\partial R(t)}{\partial x_{jk}(t)} = -\eta \{ \mu \frac{\partial H_Q(t)}{\partial Q_k(t)} B_j(t) c_{jk} + \nu \frac{\partial H_e(W_j(t))}{\partial W_j(t)} c_{jk} + \xi \frac{\partial H_s^*(t)}{\partial x_{jk}(t)} \} \\
&= -\eta \{ \mu \delta_k B_j(t) c_{jk} + \nu \frac{\partial H_e(W_j(t))}{\partial W_j(t)} c_{jk} + \xi \frac{\partial H_s^*(t)}{\partial x_{jk}(t)} \}, \\
\Delta x_{ik}(t) &= -\eta \frac{\partial R(t)}{\partial x_{ik}(t)} = -\eta \{ \mu \delta_k P_i(t) c_{ik} + \nu \frac{\partial H_e(W_i(t))}{\partial W_i(t)} c_{ik} + \xi \frac{\partial H_s^*(t)}{\partial x_{ik}(t)} \}, \\
\Delta x_{ij}(t) &= -\eta \frac{\partial R(t)}{\partial x_{ij}(t)} = -\eta \{ \mu \delta_j^* P_i(t) c_{ij} + \nu \frac{\partial H_e(W_i(t))}{\partial W_i(t)} c_{ij} + \xi \frac{\partial H_s^*(t)}{\partial x_{ij}(t)} \},
\end{aligned} \tag{6}$$

where,

$$\delta_j^*(t) \equiv \delta_j(t) + \sum_k \delta_k(t) w_{jk}(t), \delta_j(t) \equiv \frac{\partial H_B(t)}{\partial B_j(t)}, \delta_k(t) \equiv \frac{\partial H_Q(t)}{\partial Q_k(t)}.$$

2.3 Dynamic Operation of Power-Flow Control

These power nodes and the switching values can be operated in *a synchronous or asynchronous manner*, where the synchronous operation means all power nodes ($P_i(t)$, $B_j(t)$, $B_{j'}(t)$ and $Q_k(t)$) and the switching values $x_{ij}(t)$ etc. are operated

at the same time, and on the other hand, the asynchronous operation means these power nodes and the switching values are operated at any time.

The procedure for the *synchronous* updating of the values $P_i(t)$, $x_{jk}(t)$ and $x_{ij}(t)$ as follows:
(1) Randomly set the initial values of $\forall^{i,j}\ x_{ij}(t)$ between 0 and 1.
(2) Calculate the value of the objective function $R(t)$ using Eq.(4) during the forward propagation of power.
(3) Using Eq.(6), calculate the values of $\forall^{i,j}\ \Delta x_{ij}(t)$. Then, update the values of $x_{ij}(t)$ using the following equations:

$$x_{ij}(t+1) = x_{ij}(t) + \Delta x_{ij}(t).$$

(4) Using Eq.(5), update $\forall^{i}\ P_i(t)$ according to the following equation:

$$P_i(t+1) = P_i(t) + \Delta P_i(t).$$

(5) Check the termination criterion.
When the changes in power $\forall^{i}\ \Delta P_i(t)$ and the switching values $\forall^{i,j}\ \Delta x_{ij}(t)$ become stable, stop the calculation. Else, go to (2).

In the smart grid power network described in this section, it is critical that the changes in power $\Delta P_i(t)$ and switching values $\Delta x_{ij}(t)$ be updated in an *asynchronous* manner. This is because the smart grid is a *highly decentralized, parallel, distributed, autonomous* communication and processing system in which all functions of the power nodes ($P_i(t)$, $B_j(t)$, $Q_k(t)$) and interconnections ($x_{ij}(t)$) should be operated in an *asynchronous* manner.

2.4 Smart Grid Integrated into Conventional Power Network

We constructed a smart grid model which integrates some mincrogrids shown in Fig.2 into a conventional power network. This architecture is shown in Fig.7, where the conventional power network serves power energy from the power plant (shown as No.1) through several transformer substations (shown as No.2-6) to some distribution power stations (shown as No.7,8,9). In this model, each microgrid has eight power nodes which include one distribution station, four batteries or storages, and three demand nodes. The distribution station distributes power from the conventional power network to the batteries/storages and demand nodes through the interconnections between the nodes. This archtecture is hierarchical and somewhat robust because even if some interconnections are broken, the other interconnections could serve power energy to the power nodes with a bypass connection. We will show some computer-simulation experimental results supposing this kinds of situations.

3 Simulation Experiments

3.1 Experiments for MicroGrid

We performed simulation experiments both in a *synchronous* and an *asynchronous* manner under the following initial conditions: setting parameters λ

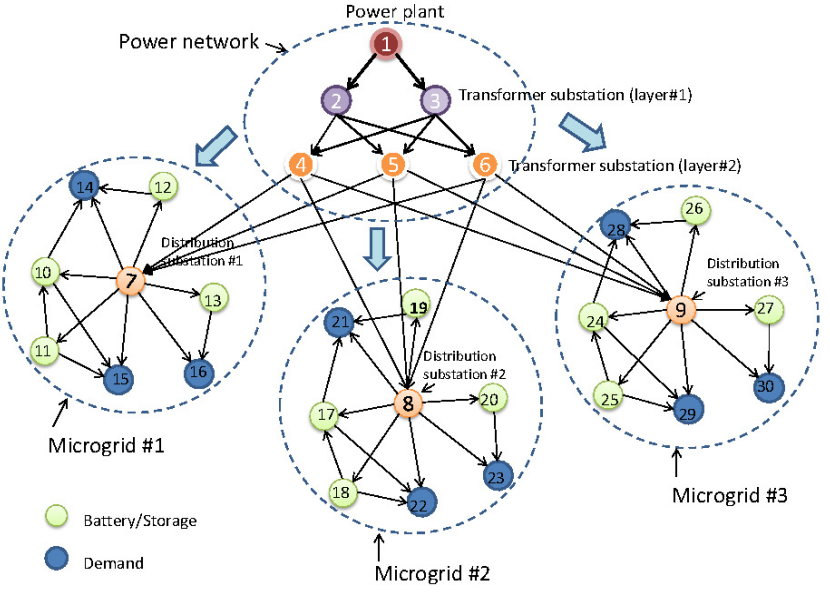

Fig. 7. Model of smart grid integrated into power network

$= \mu = \nu = \xi = 1$ for the weight of penalty, and $a_i = b_i = c_i = 1$ for simplicity in the objective function $R(t)$. $B_{min} = 0.2$, $B_{max} = 0.8$, $Q_{min} = 0.2$, and $Q_{max} = 0.8$. The power values for the transformer or distribution substation (or battery) $B_j(t)$ and the demand $Q_k(t)$ are *normalized*, and their values, in principle, are between 0 and 1. Other miscellaneous parameters are set as follows: $\alpha_p = 0.5$, $\alpha_B = \alpha_Q = 4.0$, $\beta_e = 0.05$, $\gamma_e = 0.5$, $\eta_0 = 0.01$, and $c_{ij} = c_{jk} = c_{ik} = c_{j'j} = c_{j'k} = c_{ij'} = 1.0$.

The architecture of the microgrid power network is shown in Fig.2; as an example, one power plant $P_i(t)$, four batteries $B_j(t)$, and three sites of demand $Q_k(t)$ are shown in this figure. We only show the results in an *asynchronous manner* below due to the limited space.

When an accident occurred at the 2500^{th} time-step at the interconnection $w_{ik}(t)$ in the microgrid, and power could not be supplied from the power plant node $P_i(t)$ directly, as shown in Fig.10, the power supply for the demand node $Q_k(t)$ decreased instantaneously at the 2500^{th} time-step, as shown in Fig.9, and the power supply $P_i(t)$ fluctuated slightly, as shown in Fig.8. However, except $w_{ik}(t)$, the weights increased to recover the power supply through bypass connections such as $w_{ij}(t)$, $w_{jk}(t)$, $w_{ij'}(t)$, and $w_{j'k}(t)$, as shown in Fig.10. Even in this case, the objective function $R(t)$ showed a small fluctuation, and then, converged to a stable state, as shown in Fig.11.

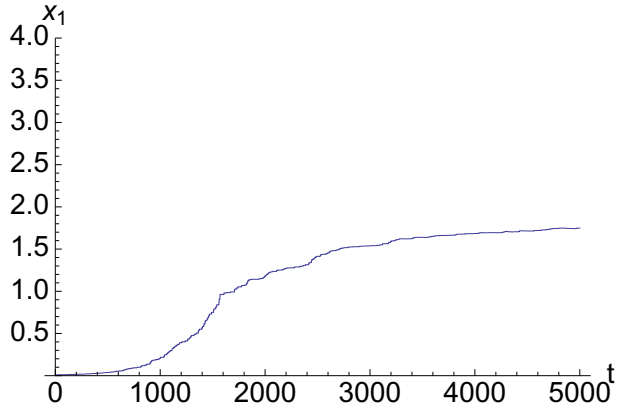

Fig. 8. Change in power $P_i(t)$ in the microgrid during a failure in an *asynchronous* manner

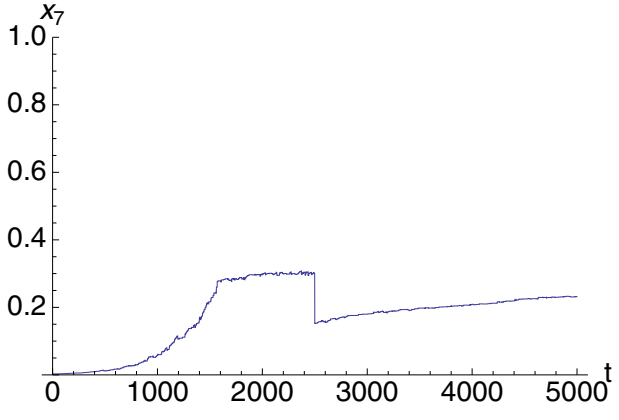

Fig. 9. Change in power at demand node $Q_k(t)$ in the microgrid during a failure in an *asynchronous* manner

3.2 Experiments for Smart Grid Integrated into Conventional Power Network

We performed simulation experiments for the architecture shown in Fig.7 both in a *synchronous* and an *asynchronous* manner under the following initial conditions: setting parameters $\lambda = \mu = \nu = 1.4$, $\xi = 1.0$ for the weights of penalty, and $a_i = b_i = c_i = 1$ for simplicity in the objective function $R(t)$. $B_{min} = 0.2$, $B_{max} = 0.8$, $Q_{min} = 0.2$, $Q_{max} = 0.8$. The power values for the transformer or distribution substation (or battery) $B_j(t)$ and the demand $Q_k(t)$ are *normalized*, and their values, in principle, are between 0 and 1. Other miscellaneous parameters are set as follows: $\alpha_p = 0.22$, $\alpha_B = \alpha_Q = 4.0$, $\beta_e = 0.05$, $\gamma_e = 0.5$, $\beta_s = 0.15$, $\eta_0 = 0.01$. We will only show the computer-simulation experimental results in an

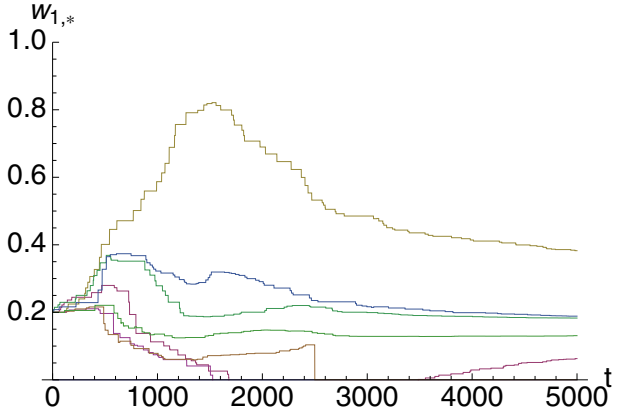

Fig. 10. Change of transmission weights $w_{ij}(t)$ in the microgrid with a failure of w_{ik} in an *asynchronous* manner

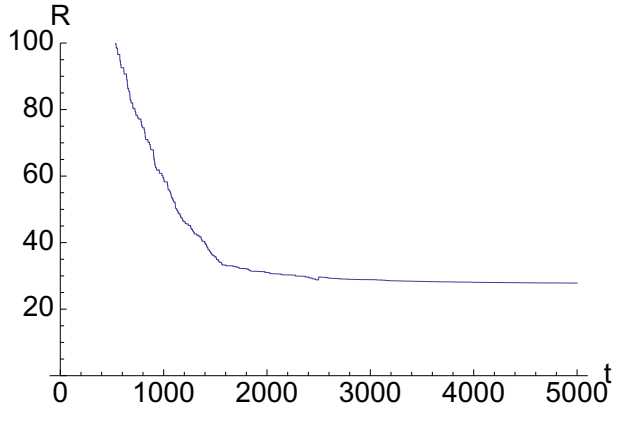

Fig. 11. Change in objective function $R(t)$ in the microgrid during a failure in an *asynchronous* manner

asunchronous manner because this manner reflects a real-world situation than the synchronous manner does.

Change in power $P_i(t)$ at power plant node, the battery node $B_j(t)$ (e.g., No.17 node), the transmission weights $w_{ij}(t)$, and the objective function $R(t)$ are shown in Figs.12, 13, 14 and 15, respectively.

The power $P_i(t)$ increased rapidly and reached a stable value of 3.8 at the 900^{th} time-step. The power of the battery node $B_j(t)$ (for example, No.17 node) increased gradually to satisfy the minimum demand value of $B_j(t)$ $(=B_j^{min})$ mostly. All the transmission weights $w_{ij}(t)$, $w_{jk}(t)$, and $w_{ik}(t)$ between the power

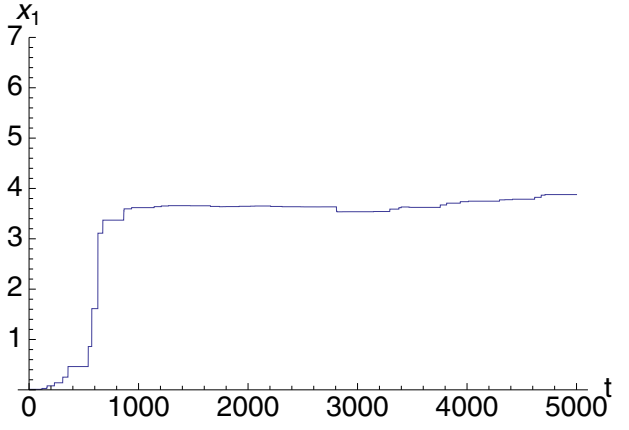

Fig. 12. Change in power $P_i(t)$ during a failure in an *asynchronous* manner

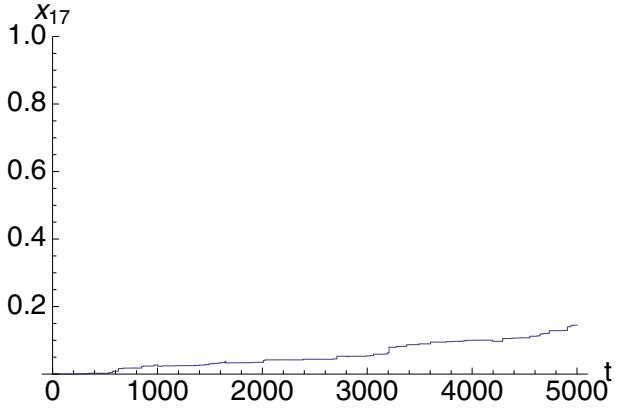

Fig. 13. Change in power at battery node $B_j(t)$ (e.g., No.17) during a failure in an *asynchronous* manner

nodes reached stable values in the range 0.0-0.25. The objective function value $R(t)$ decreased smoothly to a stable value of 150. Similarly, as in the previous subsection, when an accident occurred at the 3000^{th} time-step at the interconnection $w_{ij}(t)$ (the interconnection between No.8 and No.17), which is shown in Fig.14, and power could not be supplied from the power node directly. However, power could be supplied through bypass connections such as No.8 to No.18 and No.18 to No.17 nodes. Even in this case, the power did not fluctuate so much as shown in Fig.13, and the objective function $R(t)$ decreased as shown in Fig.15. This situation shows a *robust* feature of the smart grid shown in Fig.7.

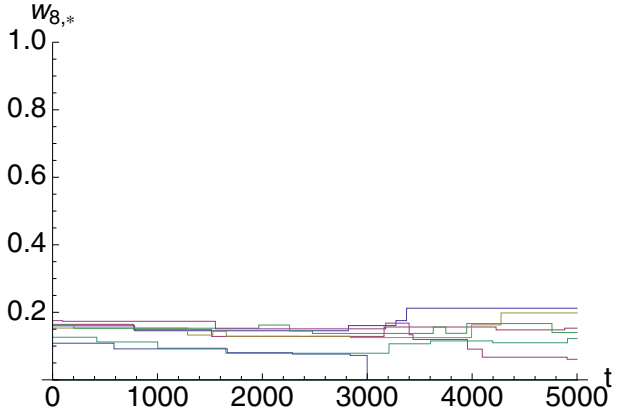

Fig. 14. Change in transmission weights $w_{ij}(t)$ during a failure of w_{ik} in an *asynchronous* manner

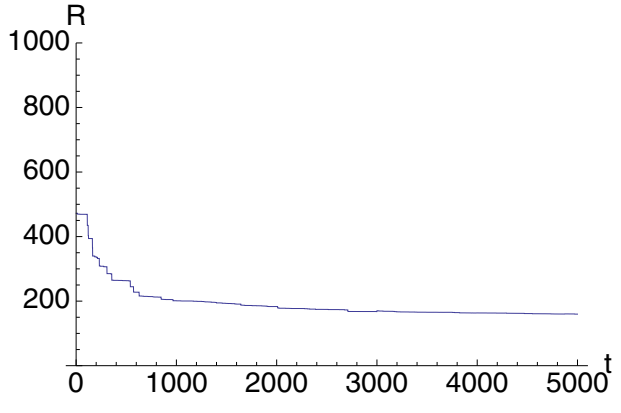

Fig. 15. Change in objective function $R(t)$ during a failure in an *asynchronous* manner

4 Discussions

We considered a smart grid and formulated the power-flow control equations when several constraints were imposed on the power plants, transformers or distribution substations, batteries/storages, and the demands. In general, the objective function is *nonlinear and time-varying*; The first term of the objective function $R(t)$ is a total fuel cost $P_0(t)$ which is a *nonlinear* term with the increase of power. The second term is $H_p^*(t)$ which is a penalty term for not decreasing the power $P_i(t)$ to zero. The third term is a constraint function which satisfies the capacity and demand in the transformer or distribution substation, and the demand, respectively. These constraint functions can be basically defined

as "well-shaped" functions shown in Figs. 4 and 5. The switching function can be defined as the function shown in Fig.6 where the switching value tends to 0(OFF) or 1(ON) as the minimum value of the function.

The minimum demand always changes with time because the demand becomes high during daytime and less at midnight. Under these conditions, the demand $D_k(t)$ is approximately represented by

$$\begin{aligned} D_k(t) =& a_k sin(\omega_k t + \theta_k) + b_k, a_k = (\epsilon Q_k^{max} - Q_k^{min})/2, \\ b_k =& (\epsilon Q_k^{max} + Q_k^{min})/2, \epsilon = 0.8, \end{aligned}$$

where a_k is the amplitude, θ_k is the phase of the k^{th} demand node, b_k is an offset with an appropriate allowance of 20% for the maximum value Q_k^{max}. When the demand $D_k(t)$ changes over time, the power-flow will change so that the objective function $R(t)$ is minimized. The smart grid can adapt to this changing environment by changing the power $P_i(t)$ as well as the switching values $x_{ij}(t)$ between all i and j nodes operating in a *highly dicentralized, parallel distributed, asynchronous and autonomous manner*. This is one of the great advantageous features for the smart grid because even if the number of power nodes increases or changes for adapting the increasing demand or the changing environment, it is unnecessary to increase the computational power for the dynamic control due to this remarkable feature.

If the battery node $B_j(t)$ belongs to the power-plant site $P_i(t)$ and the battery node $B_{j'}(t)$ belongs to the demand site $Q_k(t)$, as shown in Fig.2, the connection $w_{j'j}(t)$ can be regarded as the power-supply cable connecting $B_{j'}(t)$ to $B_j(t)$ when $B_j(t)$ has to be charged.

If the battery or demand node lacks sufficient capacity to receive power from the power plants and other batteries, the maximum capacity B_j^{max} of the battery node and Q_k^{max} of the demand node can be changed using the following equation:

$$\Delta B_j^{max} = -\eta \frac{\partial R(t)}{\partial B_j^{max}} = -\eta(\mu \frac{\partial H_B(t)}{\partial B_j^{max}}),$$

where,

$$\begin{aligned} \frac{\partial H_B(t)}{\partial B_j^{max}} =& -\alpha_B exp\{-\beta_B/(B_j(t) - \gamma_B)^2\} \\ & \times 3(B_j^{max} - B_j^{min})/\{4(B_j(t) - \gamma_B)^2\} \\ & \times [1 + (B_j^{max} - B_j^{min})/\{2(B_j(t) - \gamma_B)\}], \end{aligned}$$

Therefore, the maximum capacity B_j^{max} can be changed as follows:

$$B_j^{max} = B_j^{max} + \Delta B_j^{max},$$

Similarly, the value of Q_k^{max} in the demand node can be changed as,

$$Q_k^{max} = Q_k^{max} + \Delta Q_k^{max},$$

where,

$$\begin{aligned}
\Delta Q_k^{max} &= -\eta \frac{\partial R(t)}{\partial Q_k^{max}} = -\eta(\mu \frac{\partial H_Q(t)}{\partial Q_k^{max}}) \\
\frac{\partial H_Q(t)}{\partial Q_k^{max}} &= -\alpha_Q exp\{-\beta/(Q_k(t) - \gamma_Q)^2\} \\
&\quad \times 3(Q_k^{max} - D_k)/\{4(Q_k(t) - \gamma_Q)^2\} \\
&\quad \times [1 + (Q_k^{max} - D_k)/\{2(Q_k(t) - \gamma_Q)\}].
\end{aligned}$$

One possible way of responding to an increase in demand is to increase the capacity of power plants; however, it is very expensive to construct another power plant to meet the increased demand. On the other hand, increasing the maximum capacity of the battery and demand nodes and increasing the number of battery nodes in the smart grid are cost-effective ways to satisfy the increased demand. Furthermore, in the smart grid, the *topology of the network* can be changed by changing the switching values $x_{ij}(t)$, $x_{ik}(t)$ and $x_{jk}(t)$ to 0(OFF) or 1(ON) corresponding to the cables $w_{ij}(t)$, $w_{ik}(t)$ and $w_{jk}(t)$, respectively. This flexible function enables rapid adaptation to sudden changes in environment, such as outages due to power failures and disruptions during a disaster; this adaptation enables recovery by switching and connecting a *dead* node to an *alive* node. This is a *robust* feature of the smart grid that can adapt to a changing environment and promote the use of renewable energy rather than fossil energy. For this purpose, the formulation presented in this paper can be used to monitor the changing power balance in the smart grid when new power nodes are added by necessity.

The smart grid, which is a *highly decentralized, distributed, parallel communication and processing system*, will be realized in the near future. In this grid, a multi-agent system in which the information on switching values $x_{ij}(t)$, $x_{ik}(t)$ and $x_{jk}(t)$ will be embedded in communication packets will be important; these communication packets will serve as mobile agents and can be exchanged between the nodes in *an asynchronous* manner during communication. This situation will be realized by extending the smart grid from a local area to a societal, a national, an international, and a global network step-by-step as in the case of the Internet.

Furthermore, we can also extend this dynamic flow-control method in the smart grid for other fields such as logistics, dynamic resource (other than power) assignment and management, and network-flow control; for example, to extend it to logistics, the power nodes $P_i(t)$, $B_j(t)$ and $Q_k(t)$ can be regarded as suppliers, depots or substations, and consumers, respectively; and the interconnections $w_{ij}(t)$ can be regarded as transportation efficiency (i.e., inverse of cost).

5 Conclusions

Smart grid is a promising, highly distributed power network for promoting an effective use of natural energy by integrating it into the commercial power

networks. Inspiring from the dynamic features of biological creatures (e.g., a gene-regulatory network in the micro-level, function of brain in the meso-level, and behavior of agents in an ecosystem, etc.) we modeled an architecture of the smart grid by integrating a conventional power network and some microgrids into it, and then, defined the basic equations and operated the dynamic power-flow control through the defined objective function (Note that this is a *nonlinear and time-varying* function in general) imposing constraint (represented by the *well-shaped* constraint functions) on each power capacity.

To validate the model and behavior of the smart grid, we performed several simulation experiments including a power failure such as outage, both in *a synchronous and asynchronous manner* of operation. As a consequence, we found that the dynamic power-flow control was successfully achieved even for the case of the power failure both in the two manners.

Furthermore, the dynamic control method is applicable to other control problems such as dynamic resource assignment and management except power, logistics, network-flow control, dynamic control of traffic-flow such as railways and communication packets using the similar objective and constraint functions defined in this paper because there is inevitable constraint imposing on limited resources.

References

1. Alberts, B., et al.: Molecular Biology of the Cell, 4th edn. Garland Science (2002)
2. Bear, M.F., Connors, B.W., Paradiso, M.A.: Neuroscience: Exploring the Brain, 3rd edn. Lippincolt Williams & Wilkins Inc. (2007)
3. Clark, W., Gellings: The Smart Grid: Enabling Energy Efficiency and Demand Response. The Fairmont Press, Inc. (2009)
4. Strzelecki, R., Benysek, G. (eds.): Power Electronics in Smart Electrical Energy Network. Springer (2008)
5. Aida, et al.: The Micro Grid: For the Symbiosis of Distributed Power Supply and Power Networks, p. 29. Denki Shimbun Books (2004) (in Japanese)
6. Massoud Amin, S.: For the Good of the Grid, pp. 48–59. IEEE Power and Energy Magazine (November/December 2008)
7. Massoud Amin, S., Stringer, J.: The Electric Power Grid: Today and Tomorrow. MRS Bulletin 33, 399–407 (2008)
8. Massoud Amin, S., Schewe, P.F.: Preventing Blackouts. Scientific American, 60–67 (May 2007)
9. Massoud Amin, S.: Powering the 21st Century. IEEE Power and Energy Magazine, 96, 93, 94 (March/April 2005)
10. Jiang, Z.: Computational Intelligence Techniques for a Smart Electric Grid of the Future. In: Yu, W., He, H., Zhang, N. (eds.) ISNN 2009. LNCS, vol. 5551, pp. 1191–1201. Springer, Heidelberg (2009)
11. Molderink, A., Bakker, V., Bosman, M.G.C., Hurink, J.L., Smit, G.J.M.: Domestic Energy Management Methodology for Optimizing Efficiency in Smart Grids. In: Proceedings of IEEE Conf. on Power Technology, June 28-July 2 (2009)
12. Ma, Y., Zhou, L., Tse, N., Osman, A., Lai, L.L.: An initial study of computational intelligence for smart grid. In: Proc. of the Eighth Int. Conf. on Machine Learning and Cybernetics, Baoding, pp. 3425–3429. IEEE (2009)
13. Kupzog, F., Zia, T., Zaidi, A.A.: Automatic electric load identification in self-configuring microgrids. In: Proc. of IEEE AFRICON, pp. 1–5 (September 2009)